The Compact Muon Solenoid Experiment
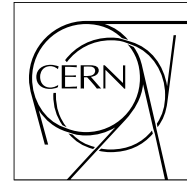
Analysis Note

The content of this note is intended for CMS internal use and distribution only

Study of Transverse Momentum Resolution in CMS Barrel Muon Spectrometer

L. Bianchini

Abstract

This work proposes an analytical study of transverse momentum resolution in the CMS muon spectrometer. The uncertainty on track momentum ($\frac{\delta p_T}{p_T}$) is calculated as the combined effect of measurement errors and Multiple Scattering. It has been obtained from a standard least squares method, i.e. by minimizing a χ^2 function of the unknown parameters. The estimator for $1/p_T$ and its variance are derived as functions of the geometric parameters and magnetic field of CMS. The result is compared to Monte Carlo prediction, and good agreement is found.

1   Introduction

Reconstruction of Monte Carlo simulated muons provides detailed measurements of p_T-resolution over the entire barrel and for a large range of momenta. In addition, muon reconstruction takes into account all possible interactions between charged particles and massive detectors (energy loss, showering, Multiple Scattering, δ-rays). Alternatively, given the geometry of the transverse plane of CMS, it is possible to determine the momentum resolution of the barrel muon system by performing a standard *least squares* calculation. Apart from MS, these effects can hardly be accounted for in a by-hand calculation. However, an analytical study is likely to give a more intuitive comprehension of how muons reconstruction job is done. The relative importance of geometric parameters to the overall resolution can be investigated. Such a calculation should give a result not too different from MC predictions, at least within the errors expected by assuming simplified geometry and by neglecting energy losses.

2   Least Squares method

The method of least squares applied to tracking in the barrel involves constructing a χ^2 function of track parameters using the measurements from the DT system, and by minimizing it with respect to its arguments. Estimators for the unknown parameters and for their covariance matrix are derived from this procedure. In order to study the contribution of the single measurements to the final resolution, we will refine progressively the fit by including at first only the angles of the segments in each muon station, then the mid-points of each segment, and, finally, the vertex constraint.

Particles tracking in a massive detector is affected by multiple scattering. Such effect has to be considered, since in CMS, tracking is done inside iron.

Tracking in the plane perpendicular to magnetic field involves fitting the trajectory to the curved path imposed by Lorentz force. In CMS, this trajectory is a piecewise curved line, consisting of circular arcs inside the return yoke (saturated by a 2 T field), connected by segments inside the stations, where magnetic stray fields can be neglected. A charged particle path between the interaction point and the coil is a circle of radius $R = p_T/0.3B$, where R is measured in meters if p_T and B are expressed in GeV/c and Tesla respectively.

In each $r - \phi$ station (at most) eight hits per muon are recorded, and we suppose that a straight line fit has been carried out, producing a measurement of angle [1] and position at the center of the station, where their errors are uncorrelated. Then, the error on the angle and position can be related to the single-point resolution σ_T of a drift tube by the relation:

$$\sigma_\phi = \frac{\sigma_T}{\sqrt{\frac{28}{9}d^2 + 4dh + 2h^2}} \tag{1}$$

$$\sigma_x = \frac{\sigma_T}{\sqrt{8}} \tag{2}$$

In (1), we have put h equal to the distance between the outermost layer of SLΦ_1 and the innermost layer of SLΦ_2 ($h \approx 21.1$ cm), and d equal to the height of one SuperLayer ($d \approx 5.2$ cm).

Suppose that a muon of a given charge has been produced in a collision and that it has gone through the barrel. Segments have been reconstructed, giving the array of measurements **y**. The trajectory of the particle can be parameterized by three parameters. A convenient choice is:

- ϕ_0: angle in MB1,

- x_0: mid-position in MB1,

- $1/p_T$: inverse of muon transverse momentum.

Measurements are actually random variables, and their mean values can be related to the above parameters. In order to keep the dependence linear, we shall assume that angles are small enough to allow first order approximation of

---

[1] Angles are measured w.r.t the same axis, which is taken to be normal to the stations. This axis is denoted by $\hat{y}$, while the axis parallel to the chambers planes is denoted by $\hat{x}$.

their trigonometric functions. Of course, the higher the momenta, the better this approximation will work. Then, we can write:

$$\mathbf{y} = H\boldsymbol{\theta} \tag{3}$$

with the H matrix given by the geometry of transverse plane and by the **B** field map, and by $\boldsymbol{\theta}$ we mean the array:

$$\begin{pmatrix} \phi_0 \\ x_0 \\ \frac{1}{p_T} \end{pmatrix}$$

By a well known derivation (which can be found in the related section of [5]), estimators for $\boldsymbol{\theta}$ and their covariance matrix U are given by

$$\hat{\boldsymbol{\theta}} = (H^T V^{-1} H)^{-1} H^T V^{-1} \mathbf{y} \equiv D\mathbf{y} \tag{4}$$
$$U = (H^T V^{-1} H)^{-1} \tag{5}$$

where V is the covariance matrix of the measurements $\mathbf{y}$. Multiple scattering introduces zero-mean random perturbation on angles and positions. After traversing a medium of thickness l, with a radiation length X_0, a $\beta = 1$ particle with momentum p (in GeV/c) and charge number $z = 1$ undergoes a projected angular deflection $\delta\phi$ and position displacement δx with variances and correlation given by:

$$\langle \delta\phi^2 \rangle = \frac{(0.0136)^2}{p^2} \frac{l}{X_0} \left(1 + 0.038 \ln\frac{l}{X_0} \right)^2 \tag{6}$$
$$\langle \delta x^2 \rangle = \frac{1}{3} \langle \delta\phi^2 \rangle l^2 \tag{7}$$
$$\langle \delta x \delta\phi \rangle = \frac{1}{2} \langle \delta\phi^2 \rangle l \tag{8}$$

As one can easily verify, $\delta\phi$ and δx are positively correlated, with correlation $\rho = \frac{\sqrt{3}}{2}$. MS introduces correlation between the measurements, resulting in a V matrix different from the diagonal one expected for N independent measurements. Once this effect has been included, the variance of (the estimator for) $1/p_T$ is given by the corresponding U element, and the relative error on p_T, indicated with $\frac{\delta p_T}{p_T}$ hereafter, can be derived from the chain:

$$\frac{\delta p_T}{p_T} \equiv \frac{\sigma(p_T)}{p_T} = \frac{\sigma(\frac{1}{p_T})}{\frac{1}{p_T}}. \tag{9}$$

Because of MS, $\mathrm{cov}\left[\frac{1}{p_T}, \frac{1}{p_T}\right]$ depends on p_T, so that momentum resolution in general does not simply scale with p_T.

2.1 Fitting angles

Suppose that only angles are measured. This situation corresponds to muons traversing a barrel wedge and being measured only there. In this case, we can compute the difference between the angles of neighboring stations $\phi_i - \phi_{i-1}$, resulting in a set of three correlated measurements. It happens however that these three measurements are *not* correlated to one another by MS, since, in making the difference, contributions from previous deflections cancel out. Only one parameter can be fitted ($\frac{1}{p_T}$). Then, the covariance matrix of the three measurements is given by[2)]

$$\begin{pmatrix} 2\sigma_\phi^2 + \sigma_{MS}^2 & -\sigma_\phi^2 & 0 \\ -\sigma_\phi^2 & 2\sigma_\phi^2 + 2\sigma_{MS}^2 & -\sigma_\phi^2 \\ 0 & -\sigma_\phi^2 & 2\sigma_\phi^2 + 2\sigma_{MS}^2 \end{pmatrix} \tag{10}$$

[2)] For simplicity, we shall assume that σ_{MS}^2 is just half the value of MS variance in the second and third iron yokes, *i.e.* we neglect the logarithmic term which violates the linear dependence on l.

while H vector is given by

$$\begin{pmatrix} 0.3Bl \\ 0.3B2l \\ 0.3B2l \end{pmatrix} \tag{11}$$

where σ_ϕ^2 and σ_{MS}^2 are respectively the square of chamber angular resolution and variance of MS projected angular distribution after crossing the distance l between MB1 and MB2 (second and third return yoke irons are taken twice larger than the first iron). By applying (4) and (6), we derive the variance of $1/p_T$ as a function of p_T.

Alternatively, we can keep four angular measurements and fit ϕ_0 and $1/p_T$ in a two parameters fit. In this case, the measurements are correlated to one another by MS:

$$\begin{pmatrix} \sigma_\phi^2 & 0 & 0 & 0 \\ 0 & \sigma_\phi^2 + \sigma_{MS}^2 & \sigma_{MS}^2 & \sigma_{MS}^2 \\ 0 & \sigma_{MS}^2 & \sigma_\phi^2 + 3\sigma_{MS}^2 & 3\sigma_{MS}^2 \\ 0 & \sigma_{MS}^2 & 3\sigma_{MS}^2 & \sigma_\phi^2 + 5\sigma_{MS}^2 \end{pmatrix} \tag{12}$$

The parameters are related to the four angles by the vector

$$\begin{pmatrix} 1 & 0 \\ 1 & 0.3Bl \\ 1 & 0.3B3l \\ 1 & 0.3B5l \end{pmatrix} \tag{13}$$

Of course, the variance of $1/p_T$ is the same as before. The first parameter is assumed to be ϕ_0, the second $1/p_T$. We choose the numerical values of the geometrical parameters to be those in the following table:

B	l	r	σ_T	σ_{MS}
2 T	0.3 m	0.4 m	150 μm	$0.0677\frac{1}{p_T}$

with p_T measured in GeV/c. The value of σ_{MS} corresponds to 20 radiation lengths. With the choice of σ_T made above, 1 becomes equal to about 0.4 mrad. Momentum resolution at low-p_T is found to be about 17%. At high-p_T, $\frac{\delta p_T}{p_T}$ is around 70%. The correlation between ϕ_0 and $1/p_T$ is found to be $\rho_{\phi_0 1/p_T} = -0.065$ at 10 GeV/c and $\rho_{\phi_0 1/p_T} = -0.755$ at 1 TeV/c. The sign of the covariance is in agreement with [4]. The error on ϕ_0 at 1 TeV/c is equal to about 0.77 mrad.

2.2   Fitting angles and positions

A much more refined resolution is expected to be obtained once mid-points are used to constrain the positions of segments. The eight measurements are parametrized by ϕ_0, x_0 and $1/p_T$, and their covariance matrix is a 8×8 (symmetric) matrix. The cov $[\phi_i, \phi_j]$ elements are as in (12). The new elements are calculated in a straightforward way:

$$cov\,[\phi_i, x_j] = \begin{pmatrix} 0 & 0 & 0 & 0 \\ 0 & \sigma_{MS}^2\left(\frac{1}{2};\frac{1}{2}\right) & \sigma_{MS}^2\left(\frac{3}{2};\frac{5}{2}\right) & \sigma_{MS}^2\left(\frac{5}{2};\frac{9}{2}\right) \\ 0 & \sigma_{MS}^2\left(\frac{1}{2};\frac{1}{2}\right) & \sigma_{MS}^2\left(\frac{5}{2};\frac{9}{2}\right) & \sigma_{MS}^2\left(\frac{11}{2};\frac{21}{2}\right) \\ 0 & \sigma_{MS}^2\left(\frac{1}{2};\frac{1}{2}\right) & \sigma_{MS}^2\left(\frac{5}{2};\frac{9}{2}\right) & \sigma_{MS}^2\left(\frac{13}{2};\frac{25}{2}\right) \end{pmatrix} \tag{14}$$

$$cov\,[x_i, x_j] = \begin{pmatrix} 0 & 0 & 0 & 0 \\ \vdots & \sigma_{MS}^2\left(\frac{1}{4};\frac{1}{2};\frac{1}{3}\right) & \sigma_{MS}^2\left(\frac{3}{4};2;\frac{4}{3}\right) & \sigma_{MS}^2\left(\frac{5}{4};\frac{7}{2};\frac{7}{3}\right) \\ \vdots & \vdots & \sigma_{MS}^2\left(\frac{11}{4};\frac{19}{2};9\right) & \sigma_{MS}^2\left(\frac{21}{4};19;18\right) \\ \vdots & \vdots & \vdots & \sigma_{MS}^2\left(\frac{45}{4};\frac{85}{2},\frac{125}{3}\right) \end{pmatrix} \tag{15}$$

4

where by r we define the height of one muon station (all stations are supposed to have the same size). For sake of brevity, by $(a;b)$ we define $ar + bl$, and by $(a;b;c)$ we define $ar^2 + brl + cl^2$. Note that to recover the full covariance matrix, one needs to add the intrinsic error of chamber spatial resolution σ_x^2 to each diagonal element. The H matrix is given by

$$
\begin{pmatrix}
1 & 0 & 0 \\
1 & 0 & 0.3Bl \\
1 & 0 & 0.3B3l \\
1 & 0 & 0.3B5l \\
0 & 1 & 0 \\
r+l & 1 & 0.3Bl\left(\frac{1}{2}r + \frac{1}{2}l\right) \\
2r+3l & 1 & 0.3Bl\left(\frac{5}{2}r + \frac{9}{2}l\right) \\
3r+5l & 1 & 0.3Bl\left(\frac{13}{2}r + \frac{25}{2}l\right)
\end{pmatrix}
\tag{16}
$$

Resolution is once again obtained by applying (4) and (6), and the result is plotted in Figure 1 together with the result from Sec. 2.1. It is worth comparing the slope of the curves, especially at high-momenta. When using the positions, the resolution is largely improved because the full lever arm of the spectrometer is used.

Momentum resolution in low-p_T region, where MS is supposed to give the dominant contribution, is roughly what one would expect from formula (21) in [4], which holds for uniform spacing between four stations (neglecting logarithm in (6)):

$$
\frac{\delta p_T}{p_T} \approx \frac{0.0136}{0.3BL}\sqrt{1.3}\sqrt{\frac{L}{X_0}}
$$

where the usual units for B and L are understood. Assuming a bending power of (1.5×2) Tm, we get a resolution of about 18%, to be compared with 15% from the complete calculation (which uses angles too). If we include the logarithmic correction to MS variance, then we get a 17% resolution. Momentum resolution at 1 TeV/c is found to be about 27%. We can compare this result with the sum in quadrature (see Sec. 3):

$$
\frac{\delta p_T}{p_T} \approx \frac{0.0136}{0.3BL}\sqrt{1.3}\sqrt{\frac{L}{X_0}} \otimes \frac{\sigma_x\sqrt{73}}{0.3BL^2}p_T
$$

where the expression on the right is derived from the exact formula (13) in [4], which has been derived assuming no MS and uniform spacing between four (position) measuring stations. By choosing the value $\sigma_x = 50\ \mu$m, we get 36% at $p_T = 1$TeV/c. The correlation between ϕ_0 and $1/p_T$ is found to be $\rho_{\phi_0 1/p_T} = -0.058$ at 10 GeV/c and $\rho_{\phi_0 1/p_T} = -0.67$ at 1 TeV/c. The sign of the covariance is in agreement with that in 2.1. The error on ϕ_0 at 1 TeV/c is equal to about 0.1 mrad, and the error on x_0 is about 50 μm.
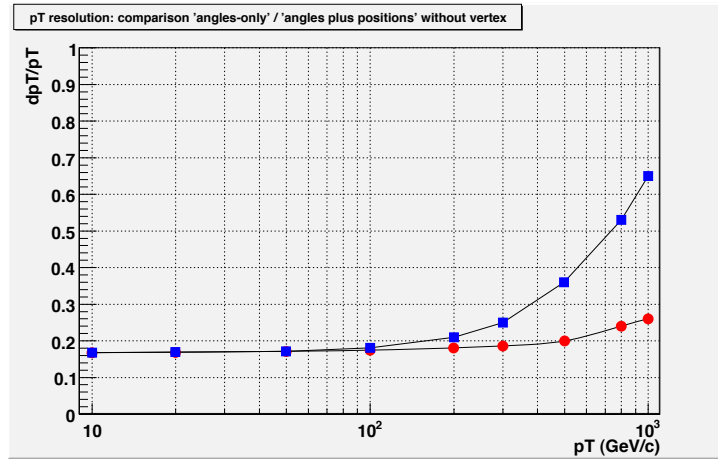

Figure 1: Comparison between p_T resolution calculated with angles only (blue) and with angles plus positions (red).

2.3 Fitting angles and positions with vertex constraint

Finally, we can add a further constraint by forcing the muon to pass through the vertex. The resolution will benefit from the huge bending power inside the coil (12 Tm). Nine measurements are available to fit three parameters. The position of the interaction point is included as a fictitious measurement, with an error equal to the transverse beam size. It is a geometrical exercise to show that, within small angles approximation, the position of the IP is given by

$$x_{IP} = x_0 - y_1\phi_0 - \frac{(0.3B_{coil}\rho^2)}{2}\frac{1}{p_T} \tag{17}$$

where y_1 is the vertical coordinate of MB1 mid-point (taking $y_{IP} = 0$), and ρ is the lever arm inside the coil, *i.e.* the length of the radius of the circle in transverse plane where magnetic field is present (we can assume that the magnetic field vanishes in the middle of the coil). The covariance matrix for the nine measurements contains correlations due to MS before MB1. These new elements are calculated in the same fashion as in (14) and (15). The new covariance matrix will be a 9×9 matrix given by the sum of the V matrix calculated in Sec. (2.2) (to which we now add a null column and row, since we include the vertex as a further measurement) and a new, say, V' matrix, which takes care of the correlations due to MS before MB1 and of the error on vertex position. We now adopt a different parametrization of V' matrix components. If we denote the average on the distribution of MS before MB1 by $\langle \cdot \rangle_{IP}$, and put $\langle \phi_1^2 \rangle_{IP} \equiv s$, $\langle x_1^2 \rangle_{IP} \equiv v$ and $\langle \phi_1 x_1 \rangle_{IP} \equiv c$, then we have:

$$cov\,[\phi_i, \phi_j]_{IP} = \begin{pmatrix} s & s & s & s \\ \vdots & s & s & s \\ \vdots & \vdots & s & s \\ \vdots & \vdots & \vdots & s \end{pmatrix} \tag{18}$$

$$cov\,[\phi_i, x_j]_{IP} = \begin{pmatrix} c & c+s(1;1) & c+s(2;3) & c+s(3;5) \\ c & c+s(1;1) & c+s(2;3) & c+s(3;5) \\ c & c+s(1;1) & c+s(2;3) & c+s(3;5) \\ c & c+s(1;1) & c+s(2;3) & c+s(3;5) \end{pmatrix} \tag{19}$$

$$cov\,[x_i, x_j]_{IP} = \begin{pmatrix} v & v+c(1;1) & v+c(2;3) & v+c(3;5) \\ \vdots & v+s(1;2;1)+c(2;2) & v+s(2;5;3)+c(3;4) & v+s(3;8;5)+c(4;6) \\ \vdots & \vdots & v+s(4;12;9)+c(4;6) & v+s(6;19;15)+c(5;8) \\ \vdots & \vdots & \vdots & v+s(9;30;25)+c(6;10) \end{pmatrix} \tag{20}$$

$$cov\,[\phi_i, x_{IP}] = 0 \tag{21}$$

$$cov\,[x_i, x_{IP}] = 0 \tag{22}$$

$$cov\,[x_{IP}, x_{IP}] = \sigma^2_{x_{IP}} \tag{23}$$

The meaning of expressions like $(a; b; c)$ and $(d; e)$ is explained above. The numerical values for s, v and c can be derived by using formula (6). We have chosen the values (p_T is measured in GeV/c):

s	v	c
0.031 $\frac{1}{p_T^2}$	0.099 $\frac{1}{p_T^2}$ m^2	0.048 $\frac{1}{p_T^2}$ m

However, because material between IP and MB1 is not homogeneous, it is not a trivial assumption that (6) still holds. Alternatively, we could make a Monte Carlo particle-gun simulation of low-p_T muons with a given momentum and (η, ϕ) direction and get s, v and c directly from the distribution of reconstructed segments in MB1.

The result of the complete calculation is plotted in Fig.2, and it has been superimposed with the curve calculated without the vertex to better visualize the change in the absolute scale of momentum resolution. We have set the new geometrical parameters to these values:

B_{coil}	y_1	ρ	$\sigma_{x_{IP}}$	$\sigma_{MS_{IP}}$
4 T	4.2 m	3.4 m	15 μm	$0.176\frac{1}{p_T}$

The value of $\sigma_{MS_{IP}}$ corresponds to 120 radiation lengths. By choosing the numerical values listed in the table, we find that momentum resolution at low-p_T is around 6.6%. This value is to be compared with what one would expect by considering only one angular measurement in MB1 with an error dominated by MS. The angle $\Delta\phi$ w.r.t the radial passing through the mid-point of MB1 segment is an estimator of $1/p_T$, since we have that:

$$\Delta\phi = \frac{0.3 B_{coil}\rho}{2}\frac{\rho}{y_1}\frac{1}{p_T} \approx \frac{1.65}{p_T}$$

However, because of MS before MB1, the x position of the segment receives random displacements, which causes the radial to be randomly reconstructed. This effect has to be taken into account, and it is easy to see that positive correlation between MS angles and displacements tends to make $\Delta\phi$ smaller. We find that the width of $\Delta\phi$ distribution is reduced by a factor $\sqrt{0.45}$ with respect to the value predicted by (6), so that:

$$\frac{\delta p_T}{p_T} = \sqrt{0.45}\frac{0.176}{p_T}\frac{p_T}{1.65} \approx 7.2\% \tag{24}$$

The difference between (24) and the 6.6% prediction from the global fit is due to the contribution of the remaining measurements in the barrel, which allow the track to be reconstructed with more precision. This can be verified by performing the following limit: let l and r tend to zero, and at the same time multiply the squares of angles and positions errors by a factor four. Then, it is as if only MB1 existed with the same nominal error. The result of this procedure predicts a 7.1% resolution.

Resolution at high-p_T is around 9.6%. This value underestimates Monte Carlo prediction by a factor ≈ 1.5. This could in part be due to a poor choice of geometrical parameters (see next paragraph). The correlation between ϕ_0 and $1/p_T$ is $\rho_{\phi_0 1/p_T} = -0.95$ at 1 TeV/c; the error on ϕ_0 is about 0.2 mrad and the error on x_0 is about 310 μm.
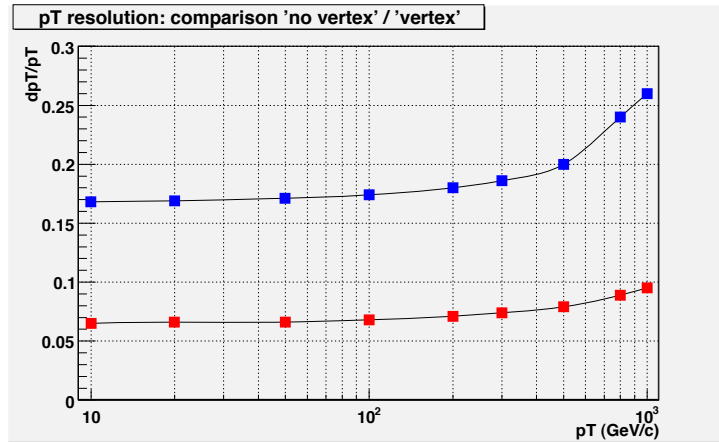

Figure 2: Comparison between p_T resolution calculated with the vertex (red) and without the vertex (blue).

3 Resolution

3.1 Analytical calculation

Momentum resolution calculated in Sec. 2.3 is a function of the geometrical parameters of the transverse plane. By varying their values, it is possible to determine their relative contribution to the overall resolution. The dependence of $\frac{\delta p_T}{p_T}$ on these parameters (magnetic field, lever arm, spatial resolution, ...) is expected to change according to

the dominant regime of momentum resolution, *i.e.* whether MS is the main source of uncertainty or if measurement error prevails. Since MS is dominant up to 200 GeV/c [2], momentum resolution at 10 GeV/c and 1 TeV/c should lie in p_T ranges characterized by different regimes.

In tracking devices, if chamber resolution is the limiting factor, then

$$\frac{\delta p_T}{p_T} \propto \frac{\sigma}{BL^2} p_T \tag{25}$$

where σ is the measurement error and L is the lever arm. If MS dominates,

$$\frac{\delta p_T}{p_T} \propto \frac{1}{B\sqrt{LX_0}}. \tag{26}$$

In general, transverse resolution in collider tracking devices is parametrised by the formula:

$$\frac{\delta p_T}{p_T} = (c_1 \times p_T) \otimes c_2 \tag{27}$$

where $\otimes$ represents the sum in quadrature of the geometrical and multiple scattering terms, and c_1 and c_2 do not depend on the momentum of the particle.

Let's now discuss how momentum resolution at 10 GeV/c (low-momentum) and at 1000 GeV/c (high-momentum) depends on few parameters.

3.1.1 Variation of the magnetic field

Momentum resolution scales with the inverse of the magnetic field (equations (25) and (26)). Since the effect of the magnetic field inside the coil is dominant, if we vary only the field inside (B_{coil}) from the nominal value of 4 T to 2 T (unrealistic scenario), then momentum resolution becomes equal to 11% and 18% respectively.

3.1.2 Spatial resolution of the chambers

At low-momentum, when MS dominates, the position error is irrelevant for momentum resolution. However, for high-momenta, $\frac{\delta p_T}{p_T}$ increases with position resolution. If the spatial error on DT single-point measurement is changed from 150 μm to 200 μm (300 μm), then momentum resolution becomes equal to 10.4% (12%), *i.e.* it increases by a relative factor 10% (30%).

3.1.3 Radius of the coil

The coil lever arm is an extremely important parameter. Suppose that ρ in equation 17 is 5% smaller than the assumption (that is, 3.2 m instead of 3.4 m). Then, $\frac{\delta p_T}{p_T}$ gets equal to 7.3% and 11% at 10 GeV/c and 1000 GeV/c respectively (*i.e.* a fractional difference of 10%). It is worth noticing that a 5% reduction in the coil radius will correspond also to a 10% decrease in the magnetic field in the iron (however, this effect gives a small correction to the values shown above).

3.1.4 Effect of the magnetic field in the iron

As an academic exercise, we can turn off the magnetic field in the iron: resolution at high-p_T gets smaller (8%). This is intuitively as if the angular and position resolution of the first chamber were increased, since the linear fit in the barrel allows a better measurement of impact (x_0) and angular (ϕ_0) parameters, which are crucial in the measurement of p_T.

3.2 Monte Carlo simulation

The analytical results of the previous Section have been compared to the Monte Carlo prediction. Samples of di-muon pairs have been generated from the IP using both CMSSW_2_0_10 and CMSSW_2_1_9. In both cases, the muons have been generated at $\eta = 0$ and flat in ϕ angle between 0 and 2π, with momenta flat in p_T in the interval

(5)10÷1000 GeV/c. A χ^2 cut on the reconstructed tracks has been applied ($\chi^2_{d.o.f} \leq 2.0$). The resolution $\frac{\delta p_T}{p_T}$ is defined as the standard deviation of the gaussian fit to the distribution of $R \equiv (1/p_T^{rec} - 1/p_T^{gen}) \, p_T^{gen}$, where p_T^{gen} is the transverse momentum generated by MC and p_T^{rec} is the value of reconstructed momentum.

3.2.1 CMSSW_2_0_10

A sample of muons tracks has been generated and reconstructed as StandAlone Muons using the version 2_0_10 of CMSSW. Muons have been reconstructed both with the vertex and without the vertex constraint. Reconstruction with the vertex has been forced by including the option *UpdatedAtVertex* in the *.cfg* file which has generated the sample. The result is shown in Fig. 3. Notice that the difference between the two plots is not as relevant as one would expect from Sec. 2.2. A cut on the number of hits has been applied to the reconstructed tracks (at least 40 hits), and the resulting curve for muons reconstructed with the vertex is compared to the resolution curve obtained without cuts (Figure 4).

The comparison between MC prediction and the analytical calculation proposed in this paper are shown in Figure 5 and 6 for muons reconstructed both with and without the vertex.
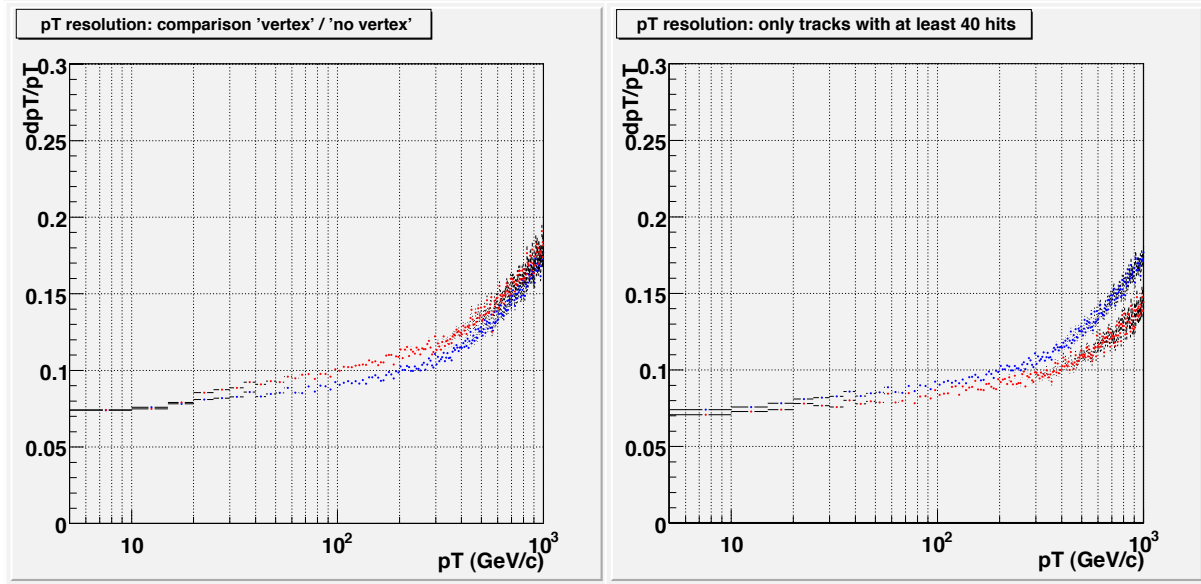

Figure 3: Momentum resolution for StandAlone muons reconstructed with (blue) and without (red) the vertex constraint using CMSSW_2_0_10.

Figure 4: Comparison between momentum resolution obtained from all tracks (blue) and momentum resolution obtained from tracks with at least 40 hits (red) using CMSSW_2_0_10.

3.2.2 CMSSW_2_1_9

A different sample of muons tracks has been generated and reconstructed as StandAlone Muons using the version 2_1_9 of CMSSW. Muons have been reconstructed both with the vertex and without the vertex constraint (Figure 7). A stronger cut has been applied to the reconstructed tracks (at least 47 hits on a maximum of 51, and four DT segments). The resulting curve has been superimposed with the resolution curve obtained without cuts (Figure 8). Momentum resolution for muons reconstructed without the vertex at low-p_T is smaller than expected from the considerations made in Sec. 2.2. The relative difference between the curves with and without cuts is not as relevant as it has been obtained using CMSSW_2_0_10. Resolution at 1 TeV/c is around 25%, while a 17% p_T-resolution was predicted by the previous version of the software.
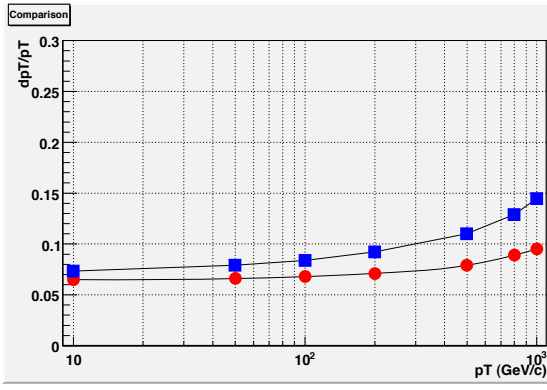
Figure 5: Comparison between p_T-resolution for muons reconstructed with the vertex using CMSSW_2_0_10 (blue boxes) and p_T-resolution from the analytical calculation in Sec. 2.3 (red points).
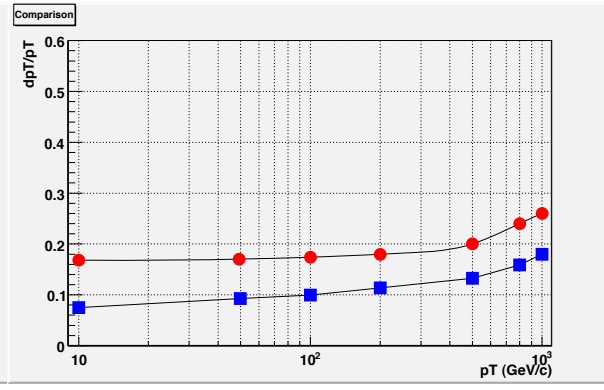
Figure 6: Comparison between p_T-resolution for muons reconstructed without the vertex using CMSSW_2_0_10 (blue boxes) and p_T-resolution from the analytical calculation in Sec. 2.2 (red points).

The comparison between MC prediction and the analytical calculation proposed in this paper are shown in Figure 9 and 10 for muons reconstructed both with and without the vertex.

4 Effect of misalignment on momentum resolution (analytical study)

In the LS method, the estimator for the unknown parameters is given by (4). Each parameter is a linear combination of the y measurements. Suppose that one chamber suffers from misalignment (bad orientation or lateral shift of the station). A systematic error is introduced, which has to be taken into account. A biased measurement changes the estimator value for $1/p_T$ by an amount proportional to the shift of the measurement. If $y_i \rightarrow y_i + \delta$, where δ can be either an angle or a position shift, then:

$$\frac{1}{p_T} \rightarrow \frac{1}{p_T} + D_{3,i}\delta \tag{28}$$

where $1/p_T$ is taken to be the third parameter. The relative systematic error on p_T is equal to the relative error on $\frac{1}{p_T}$, as in (9).

Suppose that the i-th station is rotated by $-\delta_\phi$ (angles are supposed to increase clockwise), and the muon in bending clockwise because of magnetic field. All angular measurements in MBi will be biased by $+\delta_\phi$. Taking δ_ϕ equal to 0.25 mrad (First Data Taking Scenario), we notice that the magnetic rotation $0.3Bl/p_T$ is greater then δ_ϕ up to p_T equal to 700 GeV/c, so that, for not too high momenta, the misaligned station will be more aligned with MB($i+1$) and less with MB(i-1). It turns out that if MB1 and MB2 are misaligned as described above, then the muon is reconstructed with a higher-p_T, while the opposite occurs for the other stations.

Consider now the effect of a lateral displacement of one station at the time by $-\delta_x$. It happens that such a misplacement of MB1 and MB4 causes the track to be reconstructed with a lower curvature (i.e. lower-p_T), while the opposite occurs for the other two stations.

As far the absolute scale of error is concerned, we notice that the misplacement of a station has a much more critical effect on the resolution then an angular misalignment, especially at high-p_T. Relative error on p_T remains within 1% up to 1 TeV/c for 0.25 mrad misalignment on every stations. If we put $\delta_x = 1$ mm (again, this value is taken from First Data Taking Scenario), then the systematic error for MB1 or MB4 misplacement is expected to be around 100% already at 500 GeV/c. If we displace MB2 by the same amount, the relative error exceeds 100% over about 600 GeV/c, while for MB3 the same happens over about 300 GeV/c.
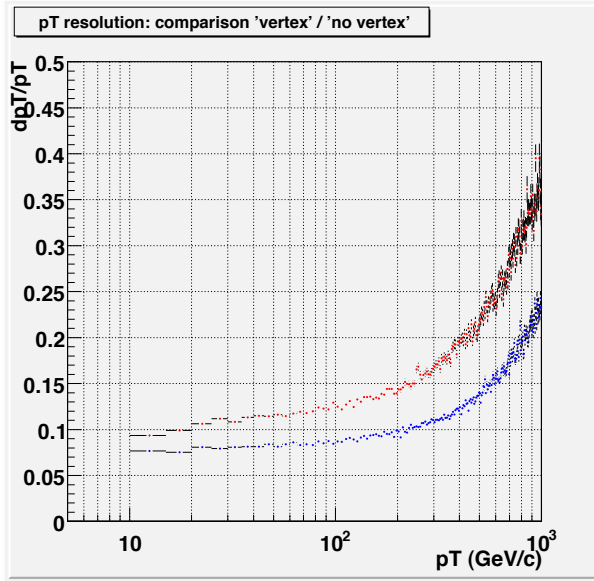
10

Figure 7: Momentum resolution for StandAlone muons reconstructed with (blue) and without (red) the vertex constraint using CMSSW_2_1_9.
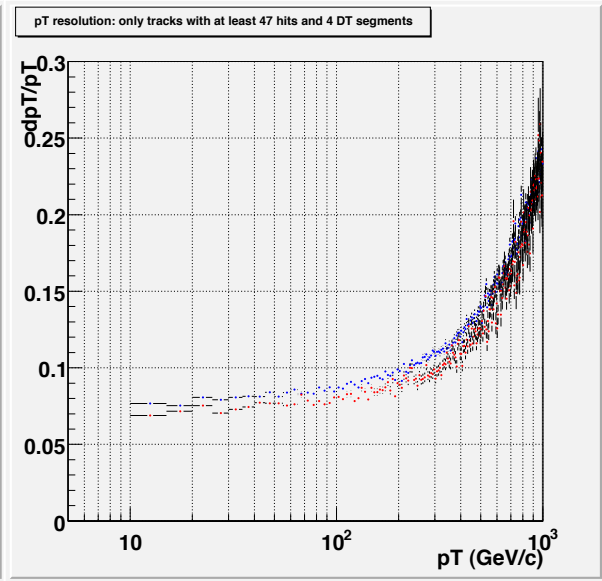
Figure 8: Comparison between momentum resolution obtained from all tracks (blue) and momentum resolution obtained from tracks with at least 47 hits and 4 DT segments (red) using CMSSW_2_1_9.
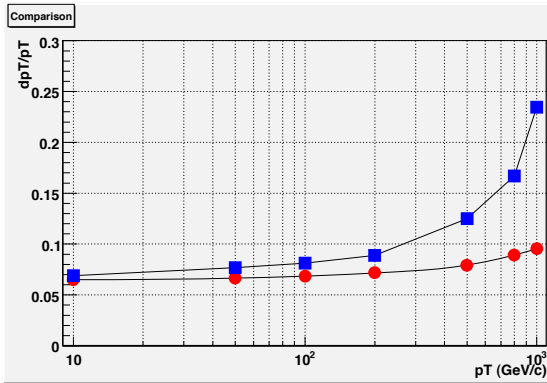

Figure 9: Comparison between p_T-resolution for muons reconstructed with the vertex using CMSSW_2_1_9 (blue boxes) and p_T-resolution from the analytical calculation in Sec. 2.3 (red points).
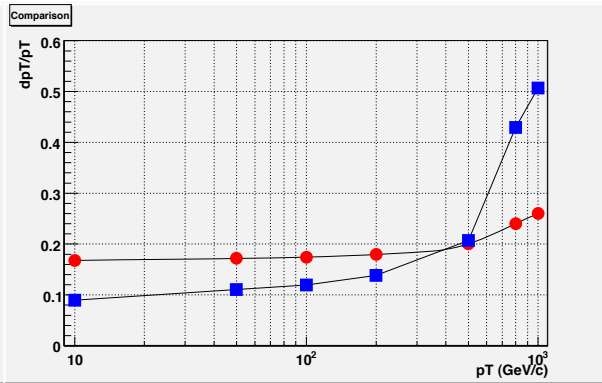
Figure 10: Comparison between p_T-resolution for muons reconstructed without the vertex using CMSSW_2_1_9 (blue boxes) and p_T-resolution from the analytical calculation in Sec. 2.2 (red points).

The shift of $1/p_T$ due to misalignment of angles and positions of the four muon stations is shown in Figure 11 and 12 for some momenta. These values are derived according to (28), with the D matrix calculated in Section 2.2.
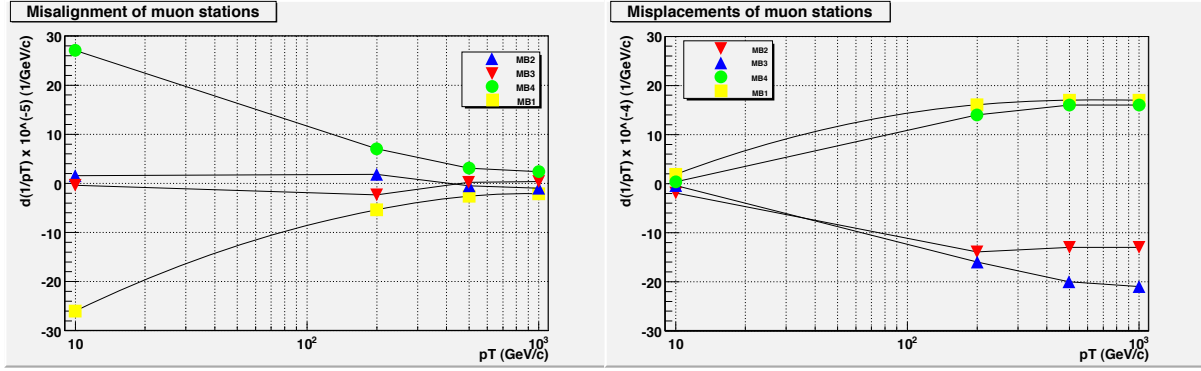

Figure 11: Shift of $1/p_T$ due to a misalignment $\delta_\phi = 0.25$ mrad of one muon station at the time.

Figure 12: Shift of $1/p_T$ due to a misplacement $\delta_x = 1$ mm of one muon station at the time.

References

[1] A. Leike. *The Phenomenology of Extra Neutral Gauge Bosons*, Phys. Rev. **317** (1999).

[2] CMS Collaboration, *Detector Performance and Software*, CERN/LHCC 2006-001, 2 February 2006.

[3] R. Tenchini, *The Physics of W and Z bosons*, World Scientific Book.

[4] R.L. Gluckstern, *Uncertainties in track momentum and direction, due to multiple scattering and measurement errors*, Nuclear Instruments and methods **24** (1963).

[5] W.M. Yao *et al.*, *Review of Particle Physics*, Journal of Physics G 33, 1 (2006).

[6] W. Blum, L. Rolandi, *Particle Detection with Drift Chambers*, Springer-Verlag (1993).

[7] CMS Collaboration, *Search for New High-Mass Resonances Decaying to Muon Pairs in the CMS Experiment*, CMS AN-2007/038, 25 January 2008.